AIAA AVIATION Forum
June 25-29, 2018, Atlanta, Georgia
2018 Applied Aerodynamics Conference

10.2514/6.2018-3632

The future of non-linear modelling of aeroelastic gust interaction

C. J. A. Wales*, C. Valente†, R. G. Cook‡, A. L. Gaitonde§, D. P. Jones¶, J. E. Cooper‖
University of Bristol, Queens Building, University Walk, Bristol, BS8 1TR

Simulation of the loads on an aircraft due to discrete '1-cosine' gusts is an import part of aircraft design and certification, as gusts often provide the critical loading cases for designing the aircraft. Due to the numerous gust cases that need to be run during a design cycle, low cost methods are preferred. Typically the Doublet Lattice Method is used due to its low cost, however it does not include transonic and viscous effects. Correction factors based of steady data are usually used to help include some of these effect. This paper looks at using a similar approach to correct the Unsteady Vortex Lattice method. In addition the correction of DLM with unsteady CFD data is also investigated. These methods are applied to a generic UAV as well as the NASA Common Research model for three different gust lengths, representative of the cases required in aircraft certification.

I. Introduction

Current trends in the commercial aircraft sector, along with environmental targets of Flightpath 2050[1], are pushing towards lighter structures and higher aspect ratios in order to produce more efficient next-generation aircraft. The result of exploring these new designs is likely to be more flexible aircraft that undergo larger deflections. Encounters with atmospheric turbulence are a vitally important consideration in the design and certification of aircraft, often defining the maximum loads that these structures will experience in service.

Non-linear coupled CFD-FEM (Computational Fluid Dynamics- Finite Element Method) simulations could bring non-linearity to the gust loads process. During each design cycle a large number of loads calculations is required even when previous experience can be used to help identify worst case gust loads. For new configurations such down selection of cases will not be possible and the costs would be prohibitively expensive.

The numerous gust cases that are required as part of the gust loads loop mean that cheap lower order methods are typically used. The existing gust loads process relies on linear assumptions which may no longer be valid as aircraft become more flexible. The current industry-standard unsteady gust load prediction is based on the Doublet Lattice Method(DLM)[2]. Being based on linearised potential flow DLM does not include thickness, transonic and viscous effects. So DLM is typically corrected with quasi-static, chord-wise integrated load distributions from wind tunnel measurements. There are a wide range of correction approaches available. They commonly rely on modifying the Aerodynamic Influence Coefficient (AIC) matrix by either multiplying or adding correction factors or even replacing the AIC matrix entirely. Traditionally these approaches have focused on providing corrections for flutter problems. Reviews of common correction approaches can be found in [3–5]. Instead of using wind tunnel data, results from the coupled CFD-FEM could be used to calculate the corrections. This allows additional unsteady data typically not available from wind tunnel testing to be used to improve the correction process; such as unsteady responses to deformations and gusts. This can be done by correcting the AIC matrices at a range of reduced frequencies to match unsteady CFD, calculated using linear frequency domain(LFD) CFD [6, 7], at a range of corresponding frequencies[8]. Alternatively a Taylor series expansion of the AIC with reduced frequency can be performed and correction matrices calculated for terms in the expansion [9].

The DLM formulation assumes small out-of-plane harmonic motions of the wing, and a flat wake. So the method is not applicable when large deformations occur. An alternative to DLM is to use the Unsteady Vortex Lattice Method (UVLM)[10] which is capable of simulating large deformations and as a result could be coupled to a geometrically

*Research Associate, Department of Aerospace
†Marie Curie Early Stage Research fellow in Aircraft Loads
‡Research Associate, Department of Aerospace
§Reader in Aerodynamics, Department of Aerospace
¶Reader in Aerodynamics, Department of Aerospace
‖Royal Academy of Engineering Airbus Sir George White Professor of Aerospace Engineering, AFAIAA, Department of Aerospace Engineering

non-linear structural model such that the aerodynamic mesh deforms with the structure. The UVLM also does not model thickness, transonic and viscous effects. However the UVLM method can also be corrected in a similar way to the DLM using static data to improve its prediction of aerodynamic non-linearities.

This paper presents work carried out as part of the EU Horizon 2020 project AEROGUST, on simulation-based gust loads process. This work will compare the aerodynamic gust loads predicted using steady corrected DLM and UVLM, as well as DLM corrected with unsteady data. The response of the models will be compared for a generic high altitude UAV wing and a transonic case for the NASA Common Research model [11]. Discrete '1-cosine' gusts, as defined in the certification requirements [12], will be the inputs used in this study.

II. Aerodynamic models

A. CFD

One of the key issues of modelling gusts using CFD is how to propagate the gust disturbance to the aircraft in an efficient manner. The gust can be applied through an unsteady farfield boundary condition. This approach requires a high mesh resolution throughout the flow domain to prevent the gust being dissipated before it can reach the aircraft. Although this method has a high cost due to the fine mesh it includes the mutual interaction between the gust and aircraft. The cost can be reduced by superimposing a fine mesh over the width of the gust. By moving this gust mesh with gust position the gust can be propagated through a coarser background mesh. This is referred to as the Resolved Atmosphere Approach (RAA)[13]. Alternatively, instead of using a fine mesh throughout the domain a higher order scheme could be used to convect the gust to the aircraft [14]. Another popular approach is to prescribe the instantaneous gust velocity throughout the computational domain which allows the gust to be convected to the aircraft on standard unsteady meshes without being dissipated. This approach is referred to as either the Field Velocity Method(FVM)[15] which is sometimes referred to as the Disturbance Velocity Approach(DVA)[13]. The drawback of this last approach is that the effect of the aircraft on the gust is not captured. A similar approach is to decompose the velocity components in to a prescribed gust component and a non gust component as follows

$$u = \tilde{u} + u_g \quad v = \tilde{v} + v_g \quad w = \tilde{w} + w_g \tag{1}$$

where u_g, v_g and w_g are the prescribed gust velocity components and $\tilde{u}$, $\tilde{v}$ and $\tilde{w}$ are the remaining velocity components. The decomposed velocities are then substituted into the Navier-Stokes equations and rearranged to solve for the non-gust components. This leads to a similar formulation to the FVM with some additional source terms. This approach is called the Split Velocity Method(SVM)[16, 17]. Due to the source terms this approach includes the effect of the aircraft on the gust.

B. Doublet Lattice Method

The DLM method is based on the integral solution of the linearised potential flow equations. The solution is obtained by integrating a kernel function that describes a periodic motion of the lifting surface. Doublet singularity elements used to describe the surface and the wake shape have fixed periodic motion. This forms the bases of the DLM developed by Albano and Rodden [2]. This leads to a linear set of equations relating the downwash induced on each panel and the pressure difference across each panel. The downwash on each panel is given by normal velocity induced by the inclination of the surface to the flow. This means that the following system of equations can be solved for the surface pressures,

$$\mathbf{C_p} = \mathbf{Aw} \tag{2}$$

where $\mathbf{C_p}$ are the pressure coefficients on the DLM panels, $\mathbf{A}$ is referred to as the Aerodynamic Influence Coefficient (AIC) matrix and $\mathbf{w}$ is the downwash vector. The forces and moments on the panel are then obtained by integrating the pressures,

$$\mathbf{F} = \mathbf{SC_p}. \tag{3}$$

where $\mathbf{F}$ are the loads and moments at the locations of interest and $\mathbf{S}$ is the integration matrix.

C. Unsteady Vortex Lattice

The UVLM solves the incompressible potential flow equations in the time domain. The surface is split up into quadrilateral elements made up of vortex line segments, forming vortex rings. At each time step, wake panels are shed

from the trailing edge elements with a circulation equal to the circulation in the shedding panel. After a fixed number of times steps the wake vortex ring elements are converted to equivalent vortex particles. The surface elements vortex strengths can be solved for by requiring that the normal velocity through the control point on each surface panel is zero,

$$\mathbf{A\Gamma} = -\left[\mathbf{U}_{wkpan} + \mathbf{U}_{wvpart} + \mathbf{U}_{\infty}(t) + \mathbf{U}_{disp}\right].\mathbf{n}_i \tag{4}$$

where n is the panel normal vector and $\mathbf{U}_{wing}$, $\mathbf{U}_{wkpan}$, $\mathbf{U}_{wvpart}$ are the velocities induced by the wing panels, wake panels and wake particles respectively. The freestream velocity is given by $\mathbf{U}_{\infty}(t)$, which can include external disturbances such as the gust input required in a gust simulation. The relative motion of the surface due to deformation is represented by $\mathbf{U}_{disp}$. With the induced velocity by the wing panels expressed in terms of the unknown panel strength, Γ_j, and $\mathbf{A}$ is the matrix of influence coefficients.

Wake

At each time step a quarter wake panel is shed from the trailing edge elements. These panels are used to enforce the Kutta condition by ensuring that the change in bound circulation on the wing is balanced by the change in circulation in the wake [18]. This is done by setting the vorticity in the first wake cell equal to the change in vorticity over the row of panels the wake panels are being shed from, which is given by

$$\left[\frac{\partial \mathbf{\Gamma}_{span}}{\partial t}\right]_{wing} = -\left[\frac{\partial \mathbf{\Gamma}_{span}}{\partial t}\right]_{wake} \tag{5}$$

The trailing edge wake panel is then shed in to the wake on the next times step. After typical two times steps, the wake panels are converted to vortex particles. The strength of the vortex particle, α, which representing the vorticity contained in a volume V can be written as

$$\alpha_p(t) = \int_{V_p} \omega(\mathbf{x}_p, t) dV_p \tag{6}$$

To avoid numerical problems, a vortex particle with a finite core is used [19] to calculate the induced velocity and is given by

$$\mathbf{u}(\mathbf{x}, t) = \frac{\rho_s\left(\rho_s^2 + \frac{5}{2}\right)}{4\pi\left(\rho_s^2 + 1\right)^{\frac{5}{2}}}\alpha_p(t) \times \hat{\mathbf{r}} \tag{7}$$

where $\rho_s = |\mathbf{r}|/\sigma$, σ is the smoothing radius, $\mathbf{r} = \mathbf{x}_p - \mathbf{x}$ and $\hat{\mathbf{r}}$ is the distance unit vector.

The vortex particles are then evolved with the local induced flow so that the force-free wake condition is satisfied. In order for the wake to be force-free, the vortex particles must be moving with the local fluid velocity [20]. In the Lagrangian reference frame, the evolution equations are solved using a forward Euler scheme, resulting in the following equation for the vortex position at discrete time (t+1)

$$\mathbf{x}_{\omega}(t+1) = \mathbf{x}_{\omega}(t) + \mathbf{u}(\mathbf{x}_{\omega}(t), t)\Delta t \tag{8}$$

and the updated vortex strength, α, is then

$$\alpha(t+1) = \alpha(t) + \nabla\mathbf{u}(\mathbf{x}_{\omega}(t), t)\Delta t \tag{9}$$

Force calculation

The incompressible unsteady Bernoulli equations can be written as

$$\mathbf{F}_i^{'} = \mathbf{F}_i - \rho_{\infty}\frac{\partial \Gamma}{\partial t}S_i \tag{10}$$

where $\mathbf{F}_i$ is the force acting on the panel, i, and $\mathbf{S}_i$ is the panel area. The first part is the steady component and the second term is the unsteady contribution to the overall force. The steady force component $\mathbf{F}_i$ can be calculated from the Kutta-Joukowski theorem given by

$$\mathbf{F}_i = \rho\mathbf{u}_i \times \mathbf{\Gamma}_i = \rho\Gamma_i\mathbf{u}_i \times \mathbf{l}_i \tag{11}$$

where $\mathbf{u}_i$ is the total induced velocity on the vortex segment, Γ is the vortex strength and $\mathbf{l}$ is the vortex leg length.

UVLM code acceleration

Since the influence on a wake particle, referred to as the target particle, is calculated using all other particles in the domain this is a problem of order $O(n^2)$. This also means the computational cost grows rapidly, as the number of particles in the wake grows with each time step. To speed up the calculation of the wake interaction, a box tree-code [21, 22] is used. An octree is constructed by repeatedly dividing the domain up into eight boxes if there are more than a set number of particles in a box, until all the particles are on the same level in the tree. To reduce the computational cost, it is possible to partition the problem into nearfield and farfield regions. In the nearfield, the influence of particles close to the target particle is calculated directly. Outside the nearfield region, particles are agglomerated together as a single particle at a higher level in the octree. As the agglomerated particles get further away from the target particle, these too are agglomerated to the next level in the octree until the penultimate level of the octree is reached. By agglomerating the particles together, the number of particle interactions that need to be calculated is reduced. Figure 1 shows the 3D boxes used to calculate the influence on a point close to the wing-tip modelled in this work. For the smallest boxes, the interactions are calculated directly, while the influence is calculated using a particle agglomerated from all the particles in the box.

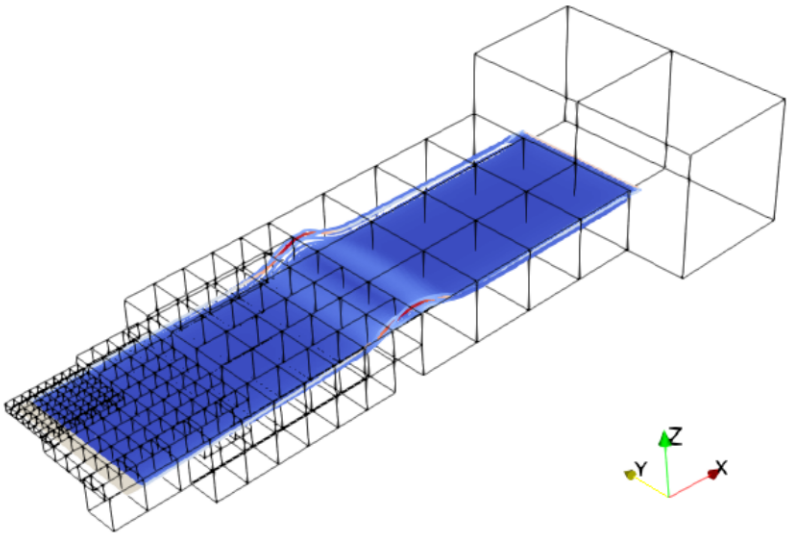

Figure 1 Octree box structure for a point close to the wing-tip. Solution show a generic UAV wing plus wake post 1-cosine gust impact.

III. Corrections

A. Steady DLM correction

The aerodynamic strip loads due to a gust disturbance calculated using the Doublet Lattice Method in NASTRAN [23] can be expressed as:

$$\mathbf{F}^{DLM} = \bar{q} w_g \mathbf{PP}(k) \mathbf{SA}^{-1} \mathbf{w}(k). \tag{12}$$

where $\bar{q}$ is the dynamic pressure, w_g is the gust scale factor, **PP** is the frequency variation in the gust, k is the reduced frequency. The aim is to correct the DLM so that sectional loads match the sectional loads calculated using CFD. This can be done in NASTRAN by supplying a downwash correction matrix. This correction matrix is calculated based on the approach found in [24] and summarised below. The steady corrected DLM strip loads are now given by,

$$\mathbf{F}^{DLM} = \bar{q} \mathbf{SA}^{-1} \mathbf{W}^{w} \mathbf{w}. \tag{13}$$

Equating the corrected DLM loads to the CFD loads results in the following equation:

$$\mathbf{F}^{CFD} = \bar{q} \mathbf{SA}^{-1} \mathbf{W}^{w} \mathbf{w}. \tag{14}$$

There is not a unique correction matrix $\mathbf{W}^w$ that will match the sectional DLM results to the CFD data. Instead, the idea is to find a correction that minimises the change to the DLM aerodynamic coefficient matrix. The aim is to produce a correction matrix as close as possible to the identity matrix. This can be done by minimising the weighted sum of the squares of the difference between the correction matrix and unity, given by:

$$\epsilon^w = \mathbf{W}^w - \mathbf{I}. \tag{15}$$

combining the above equation with equation (14)

$$\mathbf{F}^{CFD} = \bar{q}\mathbf{S}\mathbf{A}^{-1}\mathbf{I}\mathbf{w} + \bar{q}w_g\mathbf{S}\mathbf{A}^{-1}\epsilon^w\mathbf{w}. \tag{16}$$

The first term on the right hand side is the uncorrected DLM for a single gust frequency, so the above equation can be rewritten as:

$$\mathbf{F}^{CFD} = \mathbf{F}^{DLM} + \bar{q}\mathbf{S}\mathbf{A}^{-1}\epsilon^w\mathbf{w}. \tag{17}$$

Taking the difference between the CFD and DLM strip loads,

$$\Delta\mathbf{F} = \mathbf{F}^{CFD} - \mathbf{F}^{DLM}, \tag{18}$$

equation (17) can be written as

$$\Delta\mathbf{F} = \bar{q}\mathbf{S}\mathbf{A}^{-1}\epsilon^w\mathbf{w}. \tag{19}$$

The matrix ϵ^w is diagonal and $\mathbf{w}$ is a column vector. These are swapped by turning $\mathbf{w}$ into a diagonal matrix and ϵ^w into a column vector, giving

$$\Delta\mathbf{F} = \bar{q}\mathbf{S}\mathbf{A}^{-1}\mathbf{w}\epsilon^w. \tag{20}$$

In the above equation $\Delta\mathbf{F}$ is known from CFD and uncorrected DLM. The matrices $\mathbf{S}$, $\mathbf{A}^{-1}$ and $\mathbf{w}$ are known from the DLM model. This means that the correction ϵ^w can be solved for using the least squares approach.

B. Steady UVLM correction

The UVLM solves a system of equations for the circulation on a panel for a given downwash,

$$\mathbf{w} = \mathbf{A}\boldsymbol{\Gamma}, \tag{21}$$

where $\mathbf{w}$ is the downwash vector, $\mathbf{A}$ is the Aerodynamic Influence Coefficient (AIC) matrix, and $\boldsymbol{\Gamma}$ is the panel circulation. The results from the UVLM can be modified to better match experimental or CFD data by modify the downwash vector. The method used applies two correction matrices to the downwash vector leading to the new system of equations given by:

$$\mathbf{W}_0 + \mathbf{W}_w\mathbf{w} = \mathbf{A}\boldsymbol{\Gamma}, \tag{22}$$

where $\mathbf{W}_0$ is a downwash correction for the zero lift condition and $\mathbf{W}_w$ is a scaling of the down wash to correct the lift curve slope.

The relationship between the circulation and panel forces $\mathbf{f}$ can be written as:

$$\mathbf{f}^{UVLM} = \bar{q}\mathbf{Z}\boldsymbol{\Gamma}. \tag{23}$$

Combining equations (22) and (23) gives the following relationship between the downwash and the panel forces:

$$\mathbf{f}^{UVLM} = \mathbf{Z}\mathbf{A}^{-1}\mathbf{W}_w\mathbf{w} + \mathbf{Z}\mathbf{A}^{-1}\mathbf{W}_0. \tag{24}$$

The panel forces can then be integrated to give sectional loads as,

$$\mathbf{F}^{UVLM} = \mathbf{S}\mathbf{Z}\mathbf{A}^{-1}\mathbf{W}_w\mathbf{w} + \mathbf{S}\mathbf{Z}\mathbf{A}^{-1}\mathbf{W}_0, \tag{25}$$

The correction process aims to find the matrices $\mathbf{W}_0$ and $\mathbf{W}_w$ such that the theoretical sectional loads $\mathbf{F}^{UVLM}$ match the experimental or CFD loads $\mathbf{F}^{CFD}$. There are not a unique pair of matrices that can be used to correct the UVLM, so the idea is to find two matrices that minimise the change to the UVLM solution. So the aim is to find a $\mathbf{W}_0$ matrix as

close as to zero as possible and a matrix $\mathbf{W}_w$ close to the identity matrix. This can be done in the same way as the DLM. Defining difference between the CFD loads and the UVLM loads as

$$\Delta\mathbf{F} = \mathbf{F}^{CFD} - \mathbf{F}^{UVLM}, \tag{26}$$

leads to the following equation for the UVLM correction matrices,

$$\Delta\mathbf{F} = \mathbf{SZA}^{-1}\epsilon_w\mathbf{w} + \mathbf{SZA}^{-1}\mathbf{W}_0. \tag{27}$$

This results in a set of equations where there are two unknowns, ϵ_w and W_0. These means that at least two steady CFD simulations are required to solve for the correction matrices. Once again Equation (27) is solved using a least-squares approach.

The above correction method works in a single step if the downwash is fixed. However the downwash vector for the UVLM, $\mathbf{w}$, is made from two components given by

$$\mathbf{w} = \mathbf{w}_{body} + \mathbf{w}_{wake}, \tag{28}$$

where $\mathbf{w}_{body}$ is the downwash on the body due to the external flow and $\mathbf{w}_{wake}$ is the downwash due to the wake. Introducing the correction matrices changes the strength of the shed wake particles resulting in a different downwash component due to the wake. As a result the correction process has to be iterated until a set of correction matrices are found where the difference between the downwash used to generate the correction matrices and the downwash produced using the corrections is minimised.

C. Unsteady DLM correction

Instead of calculating a single correction matrix from steady data and applying it to all frequencies in DLM, separate correction matrices can be calculated for each reduced frequency, k. The DLM loads for a single frequency gust excitation are given by

$$\mathbf{F}^{DLM}(k) = \bar{q}w_g\mathbf{PP}(k)\mathbf{SA}^{-1}(k)\mathbf{w}^G(k). \tag{29}$$

The downwash due to the gust is given by

$$\mathbf{w}^G(k) = \cos\gamma e^{-i\omega(x-x_0)/U_\infty}, \tag{30}$$

were γ is the element dihedral angle, ω is the gust frequency and x_0 is the simulated gust starting position. Using unsteady CFD data, in this case from a Linearised Frequency Domain solver in the DLR-Tau code [6]. This is used to calculate the response is a sinusoidal gust, prescribed using the FVM, at each reduced frequency being corrected. Applying a correction matrix to the downwash and applying the same procedure, as in the steady DLM correction, to minimise the magnitude of the correction matrix leads to

$$\Delta\mathbf{F}^G(k) = \bar{q}\mathbf{SA}^{-1}(k)\mathbf{w}^G(k)\epsilon(k). \tag{31}$$

Defining the matrix $\mathbf{Q}$ as

$$\mathbf{Q} = \bar{q}\mathbf{SA}^{-1}(k)\mathbf{w}^G(k) \tag{32}$$

Both $\mathbf{Q}$ and ϵ are complex matrices, substituting equation 32 into equation 31 leads to

$$\Delta\mathbf{F}^G_{Re}(k) + i\Delta\mathbf{F}^G_{Im}(k) = \left[\mathbf{Q}_{Re}(k) + i\mathbf{Q}_{Im}(k)\right]\left(\epsilon_{Re}(k) + i\epsilon_{Im}(k)\right). \tag{33}$$

Expanding this equation and separating the real and imaginary parts, the correction matrices can be calculated using real arithmetic by solving the following system of equations

$$\begin{Bmatrix}\Delta\mathbf{F}^G_{Re}(k)\\ \Delta\mathbf{F}^G_{Im}(k)\end{Bmatrix} = \begin{bmatrix}\mathbf{Q}_{Re}(k) & -\mathbf{Q}_{Im}(k)\\ \mathbf{Q}_{Im}(k) & \mathbf{Q}_{Re}(k)\end{bmatrix}\begin{Bmatrix}\epsilon^G_{Re}(k)\\ \epsilon^G_{Im}(k)\end{Bmatrix}. \tag{34}$$

IV. Coupling

For aeorelastic simulations the aerodynamic model needs to be coupled with a structural model. The MSC.NASTRAN software development kit allows the development of interfaces between MSC. NASTRAN and external codes such as Tau. The OpenFSI [25] interface allows the NASTRAN to send displacements and velocities to an external code and receive back nodal forces and moments. The OpenFSi interface supports two different approaches for coupling dynamic coupling. The first is explicit coupling where the codes are loosely coupled performing one iteration per time step. The second is implicit coupling where multiple iterations are carried out per time step until the structure and aerodynamics are in equilibrium. This requires some modification to Tau to allow restarting a physical time step multiple times to enable implicit coupling. This is achieved by modifying the Tau data streams through Tau-python, see [26] for details. The same framework has been used to couple MSC.NASTRAN to the UVLM code. For the UVLM and CFD results the strong coupling has been used for the aeroelastic simulations.

V. AEROGUST Test cases

The different gust modelling techniques will be compared on a range of different configurations outlined below. In all cases a '1-cosine' gust as defined by the ESA regulations[12] is used and is given by,

$$v_g = \frac{v_{g_{max}}}{2}\left[1 - \cos\frac{2\pi(l)}{l_g}\right], \quad \text{for} \quad 0 \le l \le l_g. \tag{35}$$

where l_g is the gust length, $v_{g_{max}}$ is the gust amplitude and l is the gust penetration depth.

A. Generic UAV wing

The first test case is a generic high altitude UAV wing, designed for the AEROGUST project. The wing is unswept, untapered, with no dihedral, a span of 25 m and a constant chord of 2 m. The aerofoil section is the NASA LRN 1015 which is a 15.2% thick aerofoil. The wing has a linear twist distribution with 3° twist at the root and 0° twist at the tip, and is shown in 2. The individual wing mass is 425 kg and the full aircraft mass is 7000 kg. The wing structural model is a beam stick model designed to have a tip deflection of 1 m at trim cruise condition. The first and second bending modes occur at 1.79 Hz and 9.84 Hz respectively; the first torsion mode occurs at 15.26 Hz. The flight case for this aircraft is at Mach 0.55 at an altitude of 16 764 m . The three different '1-cosine' gust lengths used are given in Table 1.

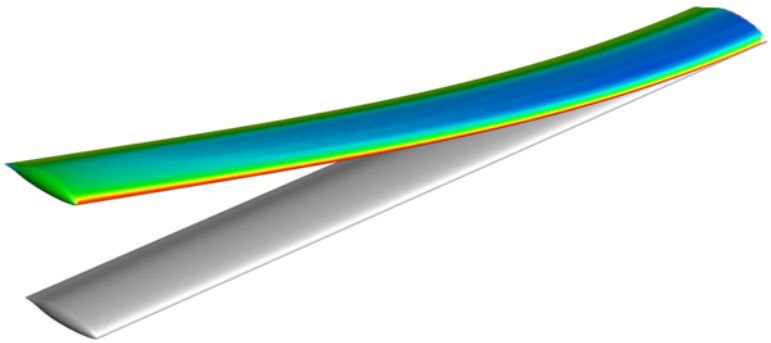

Figure 2 Generic UAV wing

Gust length(m)	Gust amplitude(m s^{-1})
18.288	11.700
91.440	15.310
213.360	17.634

Table 1 '1-cosine' gust parameters used for UAV wing

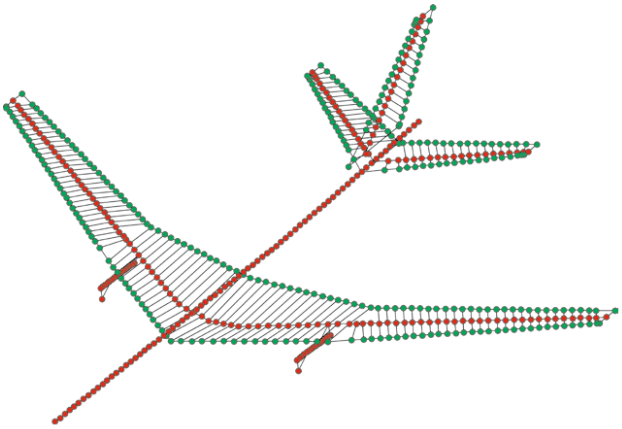

Figure 3 NCRM structural model

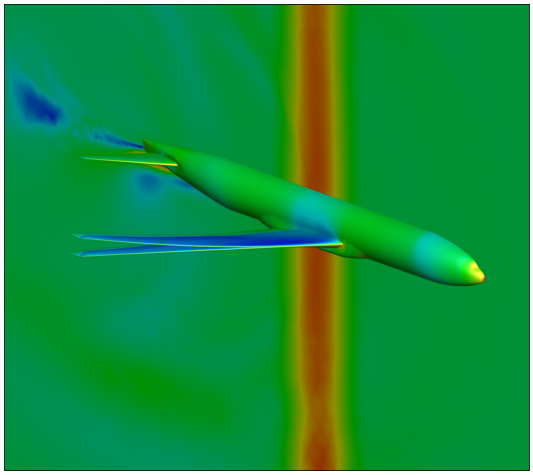

Figure 4 SVM simulation of NCRM encountering a 18.288 m **'1-cosine' gust**

B. NCRM

The third test case is the NASA Common Research Model (NCRM), which is representative of a civil airliner[11]. The structural model is a condensed beam stick model, shown in Figure 3, based on the FERMAT NCRM structural model [27]. The Maximum take off weight case (26 000 kg) was used in all analysis. For the CFD geometry, the wing body tail configuration from the 4th drag prediction work shop was used [11], as shown in Figure 4. The UVLM and DLM models used the same mesh which was based on the wing planform. The flight case for this aircraft is at Mach 0.86 and an altitude of 8839 m . The three different '1-cosine' gust lengths used are given in Table 2.

Gust length(m)	Gust amplitude(m s^{-1})
18.288	11.244
91.440	14.704
213.360	16.936

Table 2 '1-cosine' gust parameters used for the NCRM

VI. Results

A. Generic UAV wing

Both the UVLM and DLM were corrected to match static lift and pitching moments, using steady CFD data between 0° and 2°. First the corrections were applied to the rigid aerodynamic model. The change in lift coefficients for the DLM and UVLM corrected with steady data is shown in Figure 5. This shows that uncorrected DLM increasingly over predicts peak change in C_l as the gust lengths increase. This is because the wing has a high C_{l_0} and as the gusts amplitude get larger with length, the response is no longer dynamically linear. The uncorrected UVLM is much closer to the CFD results but still over predict the C_l for the longer gusts. Applying the steady correction to the DLM improves the prediction of the C_l response but it still over predicts. Applying the steady correction to the UVLM improves the prediction for the longest gust length but it now slightly under predicts the shortest two gust lengths. The results for the DLM corrected with LFD are shown in Figure 5. The unsteady corrected DLM shows excellent agreement with CFD for the shortest gust. The results for the two longer gusts also improved compared to the uncorrected DLM, however the steady corrected DLM is slightly more accurate. Next the corrected models were applied to an aeroelastic simulation for the generic UAV wing fixed at the root. The results are shown in Figure 6. These show similar trends to the rigid case.

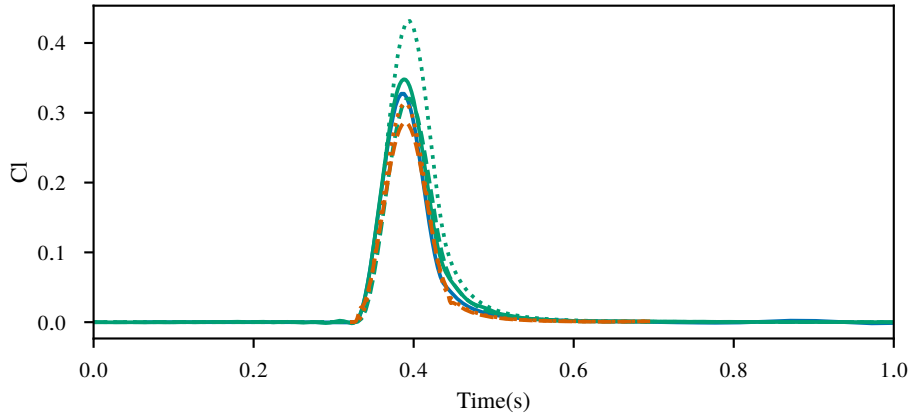

(a) 30ft gust

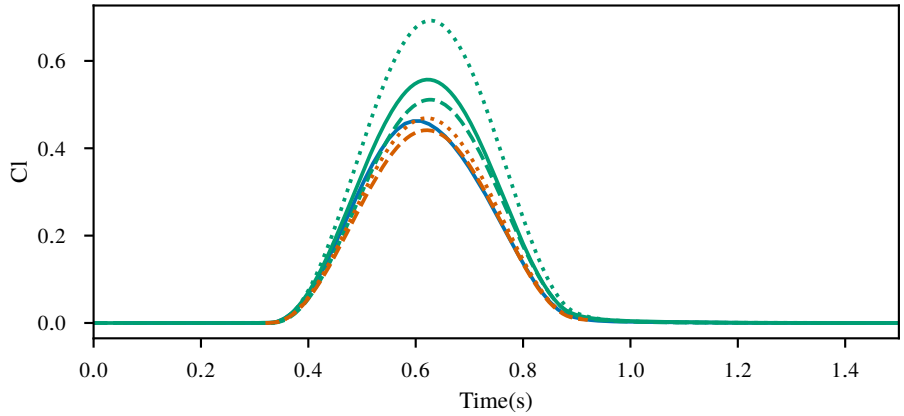

(b) 150ft gust

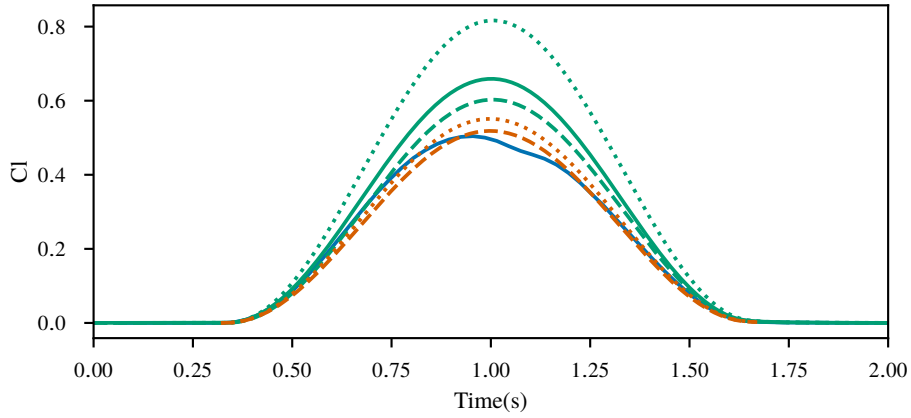

(c) 350ft gust

Figure 5 Gust response for rigid generic UAV wing

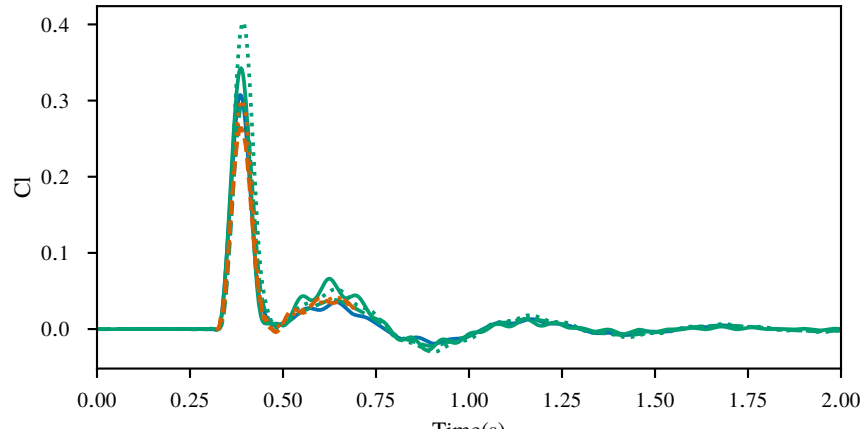

(a) 30ft gust

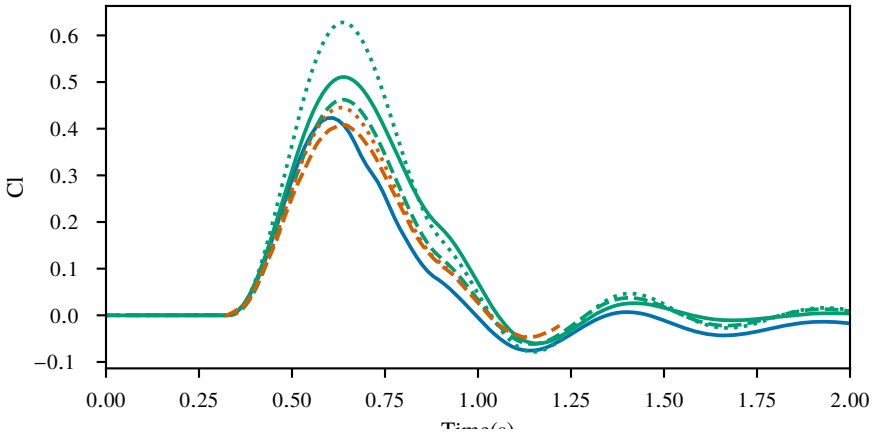

(b) 150ft gust

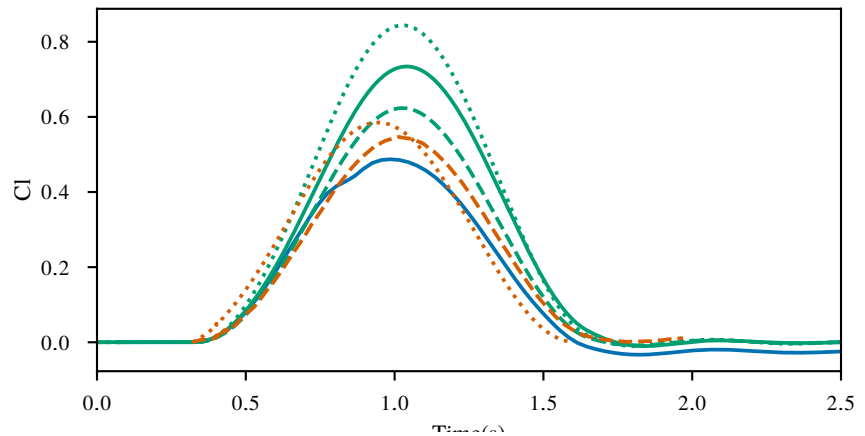

(c) 350ft gust

Figure 6 Gust response for aeroelastic generic UAV wing

B. NCRM

Both the UVLM and DLM were corrected to match static lift and pitching moments, over the wing, fuselage and HTP, using steady CFD data between 0° and 2°. The unsteady correction was preformed at 19 reduced frequencies between 0.002 and 4. First the models were compared for a rigid simulation of the NCRM, and the change in lift is shown in Figure 7. Both the uncorrected DLM and UVLM under predict the peak loads. Especially the uncorrected UVLM, this is due to the fact that it does not have any prandtl glauert correction applied, were as the DLM does model compressible effects. Applying the steady correction increases the loads predicted by both methods, with the corrected UVLM predicted the higher loads of the two methods. The UVLM shows good agreement with CFD for the shortest gust length while the corrected DLM still under predicts the loads. For the longest gust both methods over predict the loads. Using the unsteady correction improves the DLM prediction for the shortest gust as shown in Figure 7. For the two longer gusts the unsteady corrected DLM shows very similar results to steady corrected DLM.

Next the simulations were preformed for a fixed model of the NCRM with an aeroelastic wing, and the changes in C_l can be seen in Figure 8. The results show the same trend in the peak change in C_l due to the gust, as in the rigid aircraft case. The steady corrections lead to a larger aeroelastic response post gust, especially the UVLM. The unsteady corrected DLM shows a better agreement with the post gust response compared to the steady corrected DLM.

Finally, the steady correction methods were compared to a full aeroelastic simulation of the NCRM including the heave and pitch degrees of freedom. Simulations were trim by varying the angle of attack and applying a point load to the tail. Once again a similar trend in peak C_l prediction can be observed in Figure 9. The models show similar trends to the aeroelastic wing simulations, with the corrected UVLM having a larger post gust response. It can also be seen from Figure 10 that the initial climb rate is similar for all the methods, but the corrected UVLM shows a more pronounced decrease in altitude once the shorter two gusts have past, compared to the DLM and uncorrected UVLM results.

VII. Conclusions

A unsteady corrected DLM method has been compared to DLM and UVLM methods corrected using steady data, for two configurations encountering a range of discrete 1-minus cosine gusts. Correcting UVLM in a similar way to the DLM leads to improved predictions of the peak change in loads. Out of the steady correction approaches the DLM generally predicts the peak of shorter gust better while the UVLM is better for the longest gust. Correcting the DLM method using unsteady data improves the prediction of the maximum change in C_l for the shortest gust compared with the steady correction. For the longer gust for the NCRM it produces similar results to the steady correction. However, for the generic UAV wing the steady DLM correction is better for the longer gusts where the response is more non-linear. For the aeroelastic simulations the unsteady corrected DLM improved the prediction of the aeroelastic response after the gust has passed, especially for the NCRM case, while the steady corrected UVLM over predicts the post gust response.

Acknowledgements

The research leading to these results has received funding from the AEROGUST project (funded by the European Commission under grant agreement number 636053). The partners in AEROGUST are: University of Bristol, INRIA, NLR, DLR, University of Cape Town, NUMECA, Optimad Engineering S.r.l., University of Liverpool, Airbus Defence and Space, Dassault Aviation, Piaggio Aerospace and Valeol.

This work was carried out using the computational facilities of the Advanced Computing Research Centre, University of Bristol - http://www.bris.ac.uk/acrc/.

References

[1] "Flightpath 2050 Europe's Vision for Aviation," 2011.

[2] Albano, E., "A doublet lattice method for calculating lift distributions on oscillating surfaces in subsonic flows," *6th Aerospace Sciences Meeting*, No. AIAA 1968-73, American Institute of Aeronautics and Astronautics, Jan 1968.

[3] Baker, M. L., "CFD based corrections for linear aerodynamic methods," *AGARD Report*, Vol. 822, 1998.

[4] Palacios, R., Climent, H., Karlsson, A., and Winzell, B., "Assessment of strategies for correcting linear unsteady aerodynamics using CFD or experimental results," *Proceedings of the CEAS/AIAA International Forum on Aeroelasticity and Structural Dynamics*, Confederation of European Aerospace Societies, June 2001.

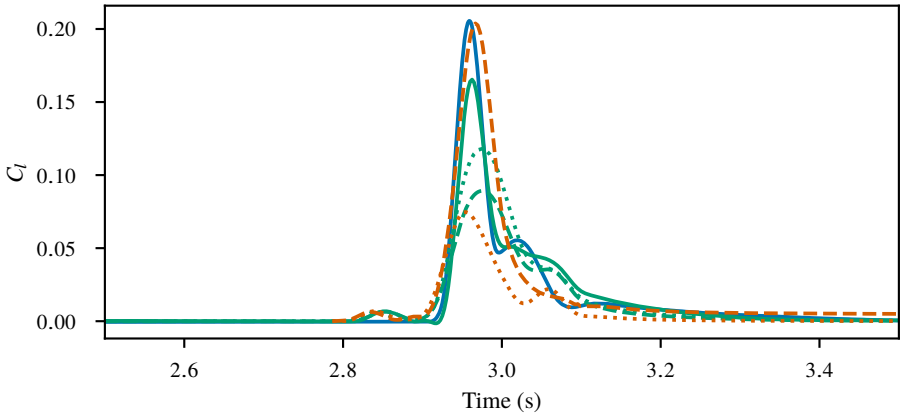

(a) 30ft gust

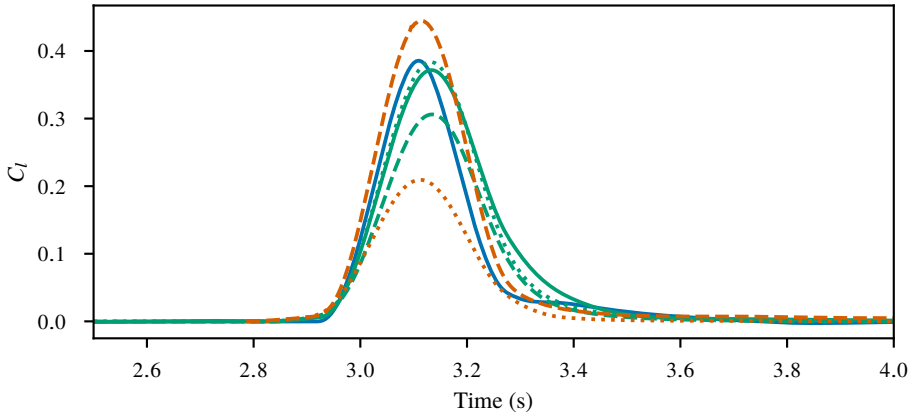

(b) 150ft gust

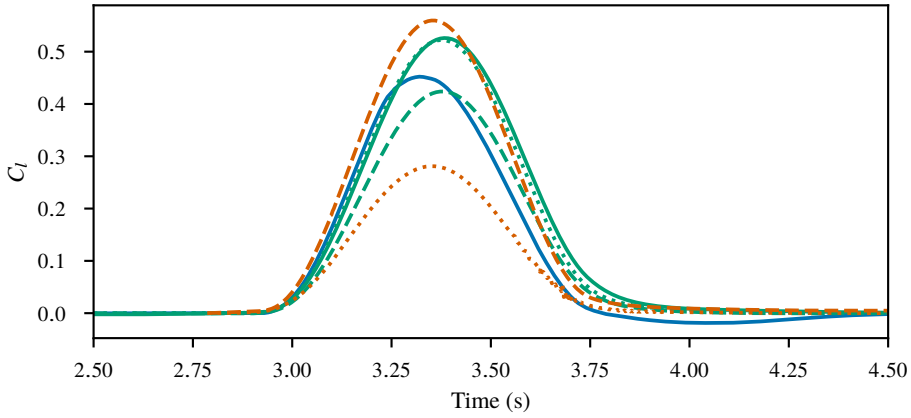

(c) 350ft gust

Figure 7 Gust response for the NCRM

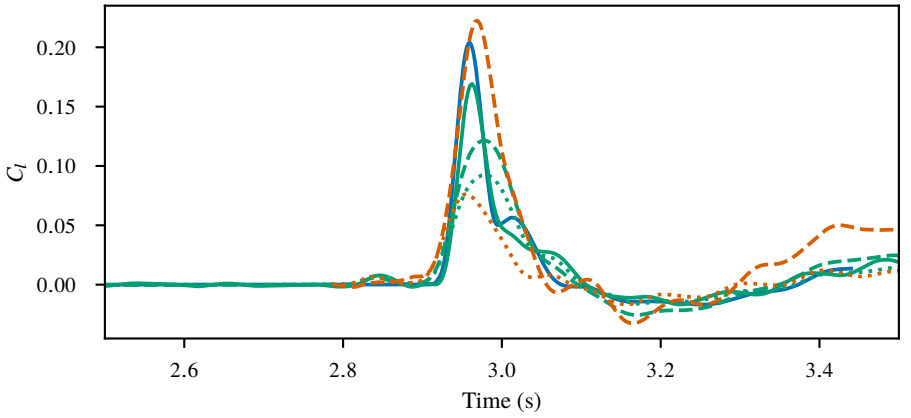

(a) 30ft gust

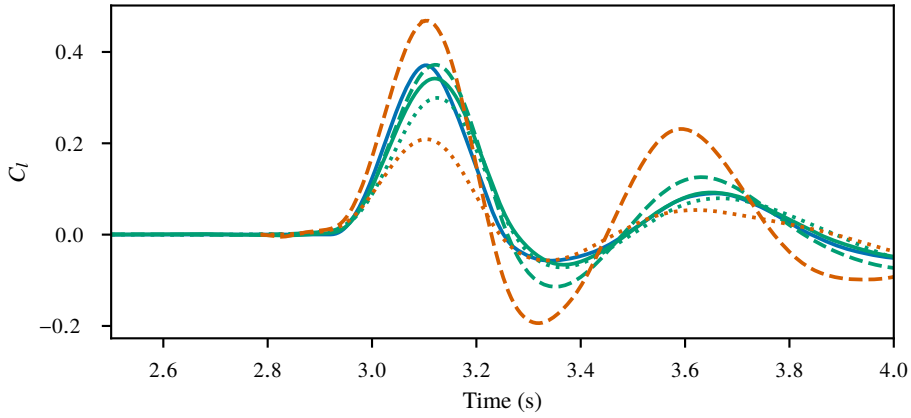

(b) 150ft gust

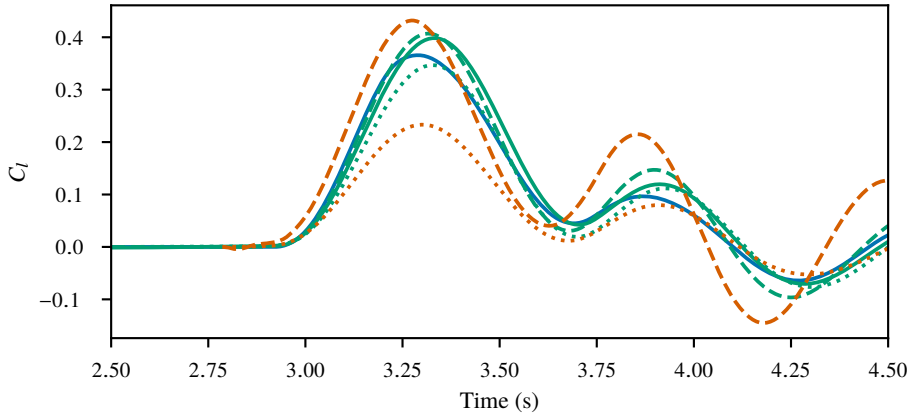

(c) 350ft gust

Figure 8 Gust response for the aeroelastic NCRM

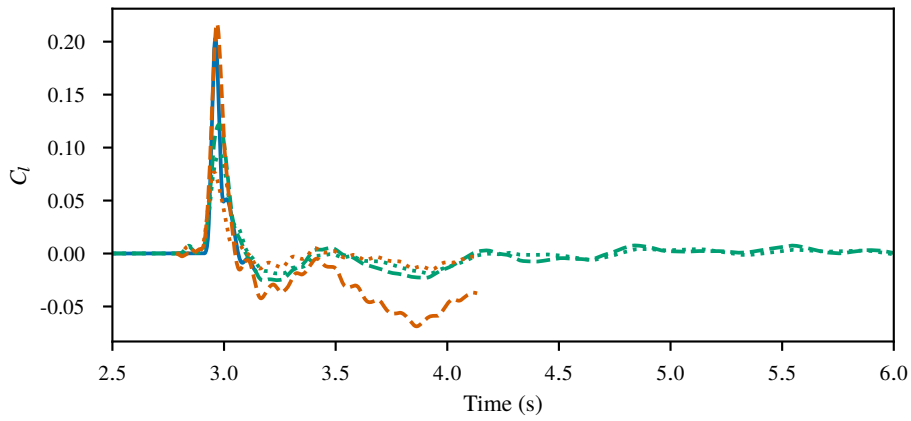

(a) 30ft gust

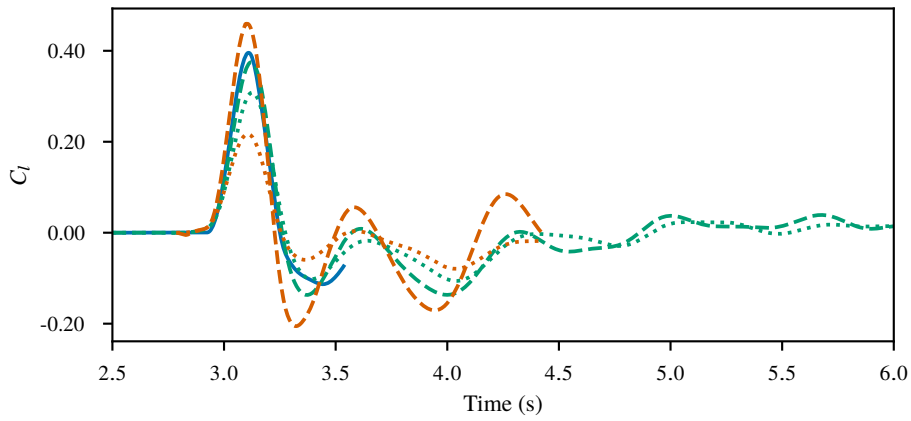

(b) 150ft gust

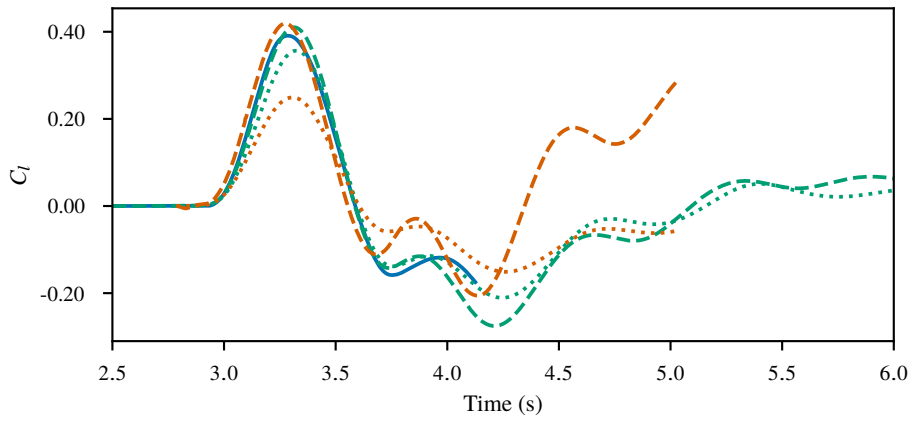

(c) 350ft gust

Figure 9 Gust response for the free air NCRM calculated using steady corrections

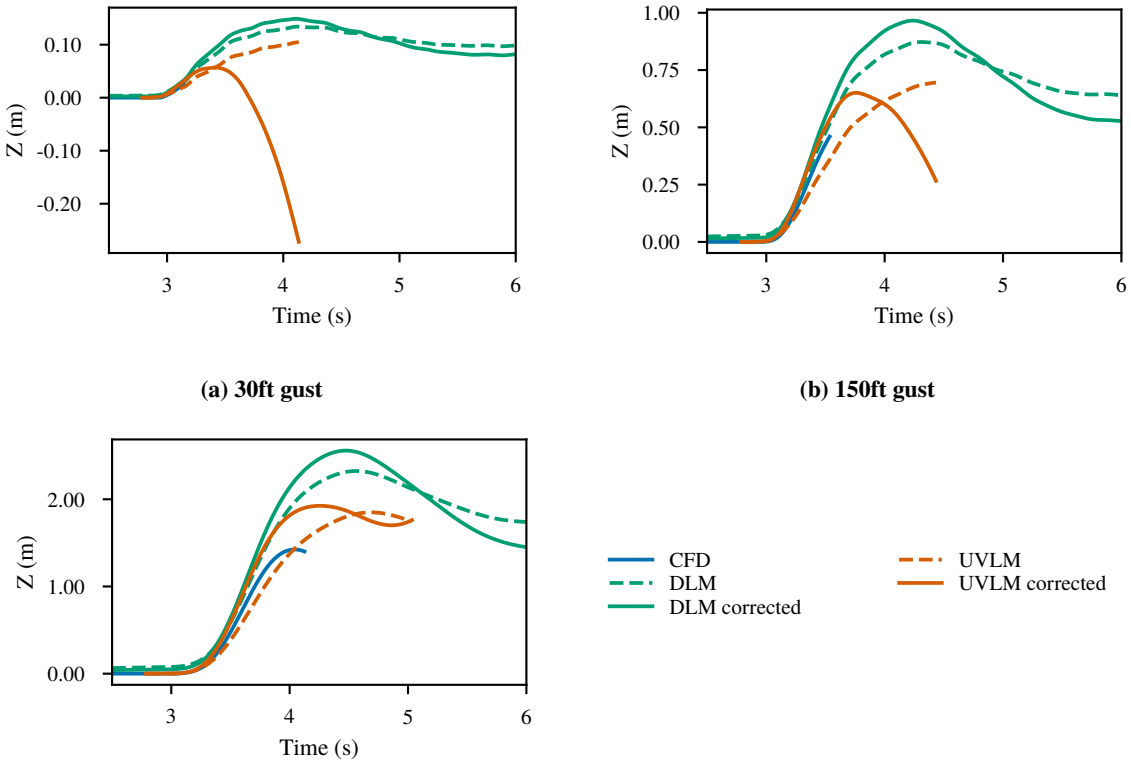

(a) 30ft gust

(b) 150ft gust

(c) 350ft gust

Figure 10 Change in altitude for the free NCRM calculated using steady corrections

[5] Silva, R. G. A., Mello, O. A. F., ao Luiz F. Azevedo, J., Chen, P. C., and Liu, D., "Investigation on transonic correction methods for unsteady aerodynamics and aeroelastic analyses," *Journal of Aircraft*, Vol. 45, No. 6, 2008, pp. 1890–1903.

[6] Bekemeyer, P., Thormann, R., and Timme, S., "Frequency-Domain Gust Response Simulation Using Computational Fluid Dynamics," *AIAA Journal*, Vol. 55, No. 7, 2017, pp. 2174–2185.

[7] Weigold, W., Stickan, B., Travieso-Alvarez, I., Kaiser, C., and Teufel, P., "Linearized Unsteady CFD for Gust Loads with TAU – IFASD 2017," *In IFASD 2017 International Forum on Aeroelasticity and Structural Dynamics*, No. IFASD 2017-187, 2017, pp. 1–15.

[8] Valente, C., Lemmens, Y., Wales, C., Jones, D., Gaitonde, A., and Cooper, J., "A Doublet-Lattice Method Correction Approach for High Fidelity Gust Loads Analysis," *58th AIAA/ASCE/AHS/ASC Structures, Structural Dynamics, and Materials Conference*, No. AIAA 2017-0632, American Institute of Aeronautics and Astronautics Inc, AIAA, 1 2017.

[9] Kaiser, C., Friedewald, D., and Nitzsche, J., "Comparison of Nonlinear CFD with Time-Linearized CFD and CFD-Corrected DLM for Gsut Encounter Simulations," *In IFASD 2017 International Forum on Aeroelasticity and Structural Dynamics*, No. IFASD 2017-101, 2017, pp. 1–16.

[10] Katz, J. and Plotkin, A., *Low-speed aerodynamics*, Cambridge university press, 2001.

[11] Vassberg, J., Dehaan, M., Rivers, M., and Wahls, R., "Development of a common research model for applied CFD validation studies," *26th AIAA Applied Aerodynamics Conference*, No. AIAA 2008-6919, 2008.

[12] "Acceptable means of compliance for large aeroplanes. CS-25. Technical report, European Aviation Space Agency," 2015.

[13] Heinrich, R., Reimer, L., and Technology, F., "Comparison of Different Approaches for Modeling of Atmospheric Effects Like Gusts and Wake-Vortices in the CFD Code Tau," *IFASD 2017*, No. IFASD-2017-091, 2017, pp. 1–13.

[14] Changfoot, D. M., *Towards a hybrid CFD platform for investigating aircraft trailing vortices*, Masters, University of Cape Town, 2017.

[15] Singh, R. and Baeder, J. D., "Generalized Moving Gust Response Using CFD with Application to Airfoil-Vortex Interaction," No. AIAA 97-2208, 1997.

[16] Wales, C., Jones, D., and Gaitonde, A., "Prescribed Velocity Method for Simulation of Aerofoil Gust Responses," *Journal of Aircraft*, Vol. 52, No. 1, 2015, pp. 64–76.

[17] Huntley, S. J., Jones, D., and Gaitonde, A., "2D and 3D gust response using a prescribed velocity method in viscous flows," *46th AIAA Fluid Dynamics Conference*, , No. AIAA 2016-4259, 2016, pp. 1–15.

[18] Willis, D. J., Peraire, J., and White, J. K., "A combined pFFT-multipole tree code, unsteady panel method with vortex particle wakes," *International Journal for Numerical Methods in Fluids*, Vol. 53, No. 8, 2007, pp. 1399–1422.

[19] Winckelmans, G. and Leonard, A., "Contributions to Vortex Particle Methods for the Computation of Three-Dimensional Incompressible Unsteady Flows," *Journal of Computational Physics*, Vol. 109, No. 2, 1993, pp. 247 – 273.

[20] Saffman, P. G. and Baker, G. R., "Vortex Interactions," *Annual Review of Fluid Mechanics*, Vol. 11, No. 1, 1979, pp. 95–121.

[21] Losasso, F., Gibou, F., and Fedkiw, R., "Simulating Water and Smoke with an Octree Data Structure," *ACM Trans. Graph.*, Vol. 23, No. 3, Aug. 2004, pp. 457–462.

[22] Selle, A., Rasmussen, N., and Fedkiw, R., "A Vortex Particle Method for Smoke, Water and Explosions," *ACM Trans. Graph.*, Vol. 24, No. 3, July 2005, pp. 910–914.

[23] MSC, *Aeroelastic Analysis User's Guide*, 2014.

[24] Giesing, J., Kalman, T., and Rodden, W. P., "Correction factory techniques for improving aerodynamic prediction methods," , No. NASA CR-144967, 1976.

[25] MSC, *MSC Software Development Kit*, 2014.

[26] Valente, C., Jones, D., Gaitonde, A., Cooper, J., and Lemmens, Y., "OpenFSI interface for strongly coupled steady and unsteady aeroelasticity," *International Forum on Aeroelasticity and Structural Dynamics*, No. IFASD 2013-178, 2015.

[27] Klimmek, T., "Development of a structural model of the crm configuration for aeroelastic and loads analysis," *In IFASD 2013 16th International Forum on Aeroelasticity and Structural Dynamics*, No. IFASD 2013-10, 2013.